An Observational Analysis of a Derecho in South China

XIA Rudi[1*] (夏茹娣), WANG Donghai[1] (王东海), SUN Jianhua[2] (孙建华),

WANG Gaili[1] (王改利), and XIA Guancong[3] (夏冠聪)

1 *State Key Laboratory of Severe Weather, Chinese Academy of Meteorological Sciences, Beijing* 100081

2 *Institute of Atmospheric Physics, Chinese Academy of Sciences, Beijing* 100029

3 *Zhongshan Meteorological Service, Zhongshan* 528400

(Received November 3, 2011; in final form June 28, 2012)

ABSTRACT

Derechos occur frequently in Europe and the United States, but reports of derechos in China are scarce. In this paper, radar, satellite, and surface observation data are used to analyze a derecho event in South China on 17 April 2011. A derecho-producing mesoscale convective system formed in an environment with medium convective available energy, strong vertical wind shear, and a dry layer in the middle troposphere, and progressed southward in tandem with a front and a surface wind convergence line. The windstorm can be divided into two stages according to differences in the characteristics of the radar echo and the causes of the gale. One stage was a supercell stage, in which the sinking rear inflow of a high-precipitation supercell with a bow-shaped radar echo induced a Fujita F0 class gale. The other stage was a non-supercell stage (the echo was sequentially kidney-shaped, foot-shaped, and an ordinary single cell), in which downbursts induced a gale in Fujita F1 class.

This derecho event had many similarities with derechos observed in western countries. For example, the windstorm was perpendicular to the mean flow, the gale was located in the bulging portion of the bow echo, and the derecho moved southward along with the surface front. Some differences were observed as well. The synoptic-scale forcing was weak in the absence of an advancing high-amplitude midlevel trough and an accompanying strong surface cyclone; however, the vertical wind shear was very strong, a characteristic typical of derechos associated with strong synoptic-scale forcing. Extremely high values of convective available potential energy and downdraft convective available potential energy have previously been considered necessary to the formation of weak-forcing archetype and hybrid derechos; however, these values were much less than 2000 J during this derecho event.

Key words: derecho, supercell, downburst, windstorm

Citation: Xia Rudi, Wang Donghai, Sun Jianhua, et al., 2012: An observational analysis of a derecho in South China. *Acta Meteor. Sinica*, **26**(6), 773–787, doi: 10.1007/s13351-012-0608-z.

1. Introduction

Derecho, a Spanish word introduced as a meteorological term by Hinrichs (1888), refers to a type of severe convective events that produce widespread and long-lived straight-line windstorms. Squall lines, bow echo systems, and supercells can all induce derechos. Johns and Hirt (1987) established criteria for distinguishing derechos from other severe windstorms (Table 1). These criteria have since been adopted either directly or with slight adjustment by a number of scholars (Bentley and Mote, 1998; Evans and Doswell III, 2001; Gatzen, 2004; Coniglio and Stensrud, 2004; Ashley et al., 2005).

Johns and Hirt (1987) divided 70 derechos into two categories: progressive derechos and serial derechos. Some derechos have characteristics of both types but are nevertheless assigned to only one category. The squall line systems that produce progressive derechos are oriented nearly perpendicular to the mean airflow, and often contain downbursts in the bulging part of the squall line system. A series of line-shaped echoes or bow echoes can also induce a progressive derecho. The squall line systems producing serial derechos are

Supported by the National Natural Science Foundation of China (41040037 and 41205028) and Basic Research Program of the State Key Laboratory of Severe Weather, Chinese Academy of Meteorological Sciences.

*Corresponding author: xiard@cams.cma.gov.cn.

Table 1. Criteria proposed to distinguish derechos from other severe windstorms (Johns and Hirt, 1987)

Number	Criteria
(1)	There must be a concentrated area of reports consisting of convectively induced wind damage and/or convective gusts > 26 m s^{-1} (50 kt). This area must have a major axis length of at least 400 km (250 nm).
(2)	The reports within this area must also exhibit a nonrandom pattern of occurrence. That is, the reports must show a pattern of chronological progression, either as a singular swath (progressive) or as a series of swaths (serial).
(3)	Within the area there must be at least three reports, separated by 64 km (40 nm) or more, of either F1 damage and/or convective gusts of 33 m s^{-1} (65 kt) or greater.
(4)	No more than 3 h can elapse between successive wind damage (gust) events.
(5)	The associated convectively induced system, as indicated by surface pressure and wind fields, must have temporal and spatial continuity. However, movement of radar echoes associated with the system need not be continuous.
(6)	Multiple swaths of wind damage (including gusts) must be a part of the same mesoscale convective system as indicated by the National Weather Service radar summary charts.

oriented at smaller angles relative to the mean airflow, and downbursts are typically located on the north side of the squall line system. The scale of serial derechos is often larger than the scale of progressive derechos.

Evans and Doswell III (2001) divided derechos into three categories according to synoptic conditions: weak-forcing, strong-forcing, and hybrid derechos. A strong-forcing derecho is situated ahead of a middle troposphere trough and accompanied by surface cyclones. A weak-forcing derecho is associated with a stronger lower tropospheric inflow and cold pool, similar to a progressive derecho. The convective available potential energy (CAPE) and downdraft convective available potential energy (DCAPE) associated with a weak-forcing derecho are higher than those associated with a strong-forcing derecho. The values of CAPE and DCAPE associated with a hybrid derecho are intermediate between the other two types.

Derechos occur frequently in Europe and the United States (Gatzen, 2004; Bentley and Mote, 1998; Coniglio and Stensrud, 2004). By contrast, reports of derechos in China are scarce, although some previous convective windstorms may have reached the criteria. The reason may simply be that this nomenclature has not yet been used in China. A number of studies have focused on squall lines or bow echoes in China (e.g., Yao et al., 2008; Chen et al., 2009; Sun et al., 2011; Wang et al., 2011), both of which are capable of producing derecho events.

Widespread heavy rainfall, hail, and thunderstorms occurred over Guangdong Province in China during 0000–0600 UTC 17 April 2011. Hail was observed sequentially in Foshan, Guangzhou, and Zhaoqing in Guangdong Province. Automatic weather stations in both Foshan and Guangzhou recorded wind gusts greater than 42 m s^{-1}, the strongest gusts observed since the automatic weather stations began taking measurements in 1994. In this event, gales (wind gusts > 17 m s^{-1}) persisted for 6 h between 0000 and 0600 UTC on 17 April, with the major axis length measuring approximately 350 km (Fig. 1). Note that the main echo moved over the ocean after 0700 UTC; due to an inability to obtain additional measurements over the ocean, it is difficult to determine whether strong winds continued, but the weakening of the radar echo after 0700 UTC suggests a weakening of wind speeds. Strong gales (gusts > 23 m s^{-1}) lasted 5 h and traveled approximately 280 km. Whole gales (gusts $>$ 26 m s^{-1}) occurred in two time periods with a 1-h interlude, lasting a total of 4 h. Gusts during the first period reached a Fujita class of F0 (18–32 m s^{-1}), but the strongest gusts occurred during the second period (0500–0600 UTC), when winds reached a Fujita class of F1 (33–50 m s^{-1}) (Fujita, 1981). The gales progressed in the same direction as the movement of the windstorm (Fig. 2), and are primarily characterized by damaging straight-line winds.

The windstorm was produced and maintained by the same mesoscale convective system throughout its existence (Fig. 3); this system is called a derecho-producing mesoscale convective system (DPMCS).

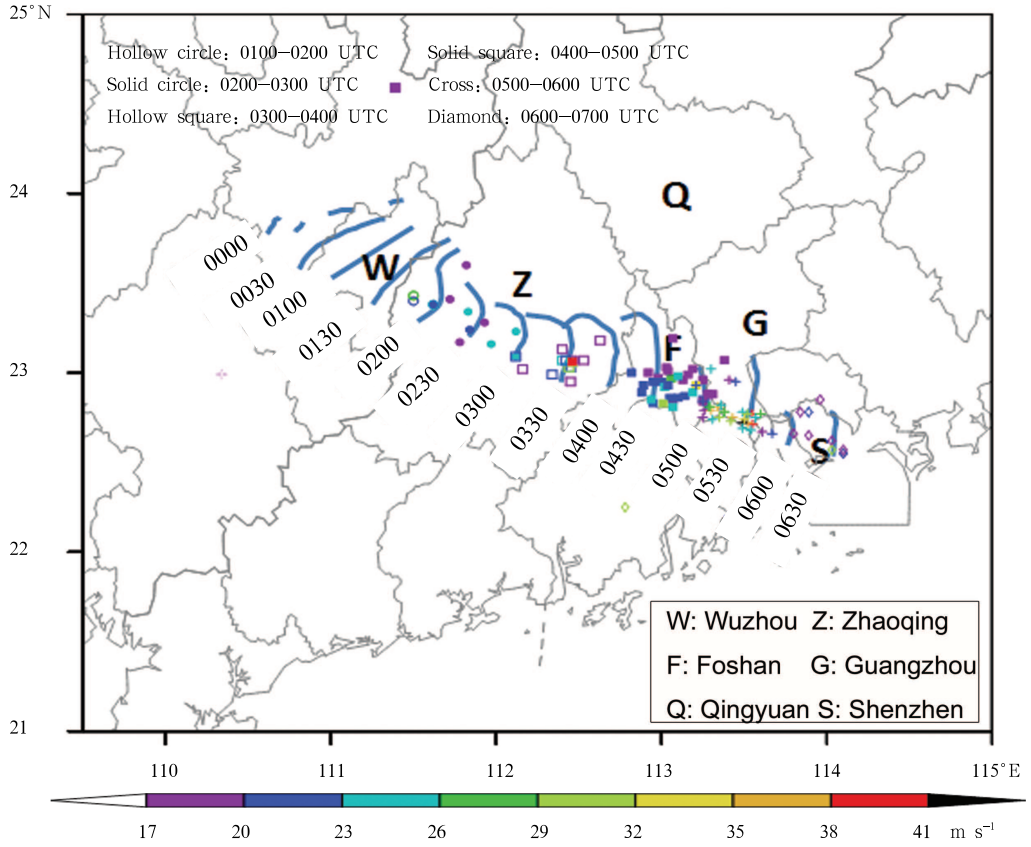

Fig. 1. Radar-observed positions of the central axis (blue line) of the area of strong echo (radar reflectivity factor $\geqslant$ 45 dBZ) at 30-min intervals between 0000 and 0630 UTC 17 April 2011. The symbols represent gusts ($\geqslant$ 17 m s^{-1}), with different colors representing different wind speeds and different symbols representing different times.

The magnitude of the strong radar echoes (SRE; radar reflectivity factor > 45 dBZ) that were associated with the windstorm changed only slightly during its duration, but the morphology of the SRE area experienced a series of substantial changes (Fig. 4). The windstorm moved southeastward in tandem with the DPMCS (Figs. 1 and 3). Although this event did not meet criterion (1) in Table 1 (because the path of gusts larger than 26 m s^{-1} was less than 400 km), it met criteria (2) through (6) in Table 1 and had the classic characteristics of derechos. We thus consider this windstorm to be a derecho event.

This event affected 2155 people, injured 153 people, and killed 17 people. The characteristics and causes of the DPMCS in this event should be investigated to enrich our knowledge about derechos in China and improve future forecasts of similar events. In this paper, the characteristics of the derecho on 17 April 2011 in South China are studied by analyzing observational data from multiple platforms, with an emphasis on the characteristics of the windstorm and the environment in which it formed. This event is compared and contrasted with derechos observed in Europe and the United States.

The data employed in this study include conventional surface and sounding observations, automatic station observations, Doppler weather radar data, and FY-2E satellite observations. These datasets have been provided by the National Meteorological Information Center and the National Satellite Meteorological Center in China. The remainder of this paper is arranged as follows: the characteristics of the DPMCS as observed by the FY-2E satellite and radar stations in South China are analyzed in Section 2, the forma-

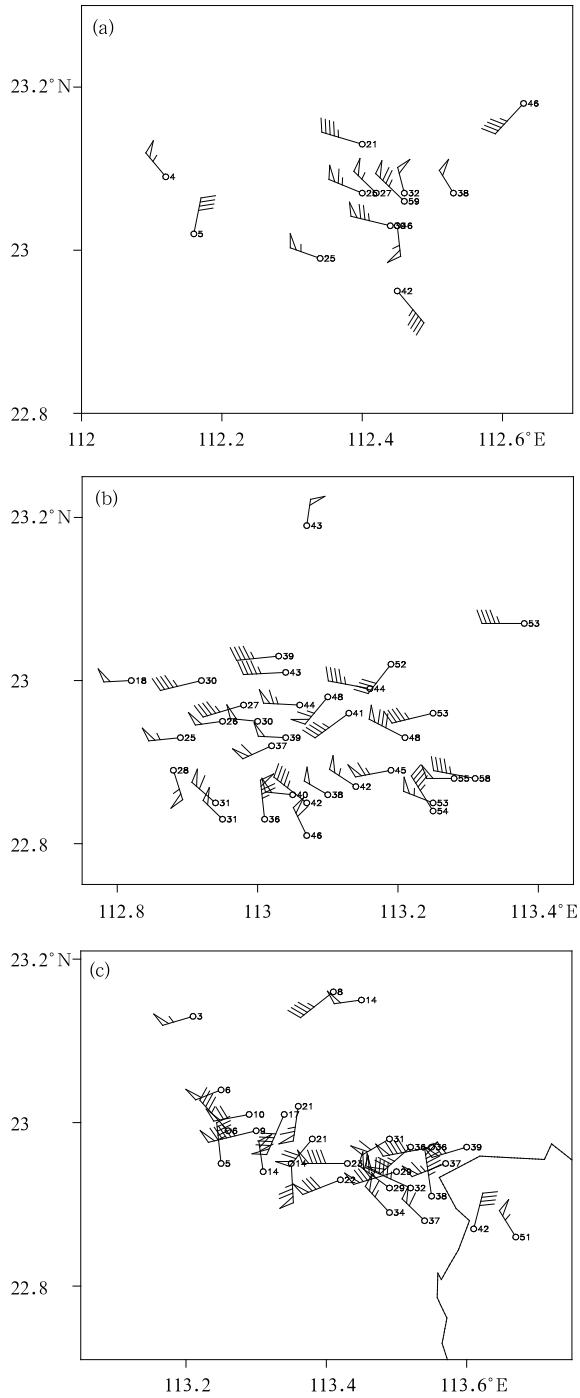

Fig. 2. Distributions of gusts ($\geqslant$ 17 m s^{-1}) at (a) 0300 UTC, (b) 0400 UTC, and (c) 0500 UTC 17 April 2011. The digits represent the occurrence times of the gales to the nearest minute.

tion and maintenance of the gales during different stages are examined in Section 3, the environmental conditions contributing to the windstorm are discussed in Section 4, and conclusions and discussion are provided in Section 5.

2. Observational characteristics of the DPMCS

Infrared images (figure omitted) illustrate that a DPMCS existed at 1900 UTC 16 April 2011. At this initial stage, the DPMCS was located to the north of a decaying meso-α-scale convective system in the middle and north of Guangxi Region. The horizontal scale of the DPMCS was approximately 40 km at this stage. At 2300 UTC 16 April 2011, the cloud top height of the DPMCS increased and its horizontal scale expanded to approximately 200 km.

During the development of the DPMCS, the western edge of the DPMCS had a clear boundary and shadow, while the northeastern edge had thread-like outflows (Fig. 3). This phenomenon indicates that the cloud top was higher and the convection was stronger in the western part of the system. The shadow indicates attenuation of solar radiation. The configuration of the system also indicates that the mean flow was

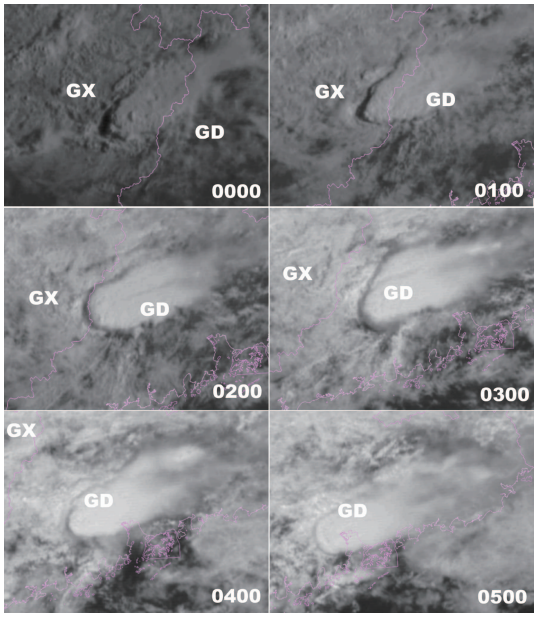

Fig. 3. Visible satellite images from 0000 to 0500 UTC 17 April 2011 observed by the FY-2E satellite. GX means Guangxi Region and GD denotes Guangdong Province.

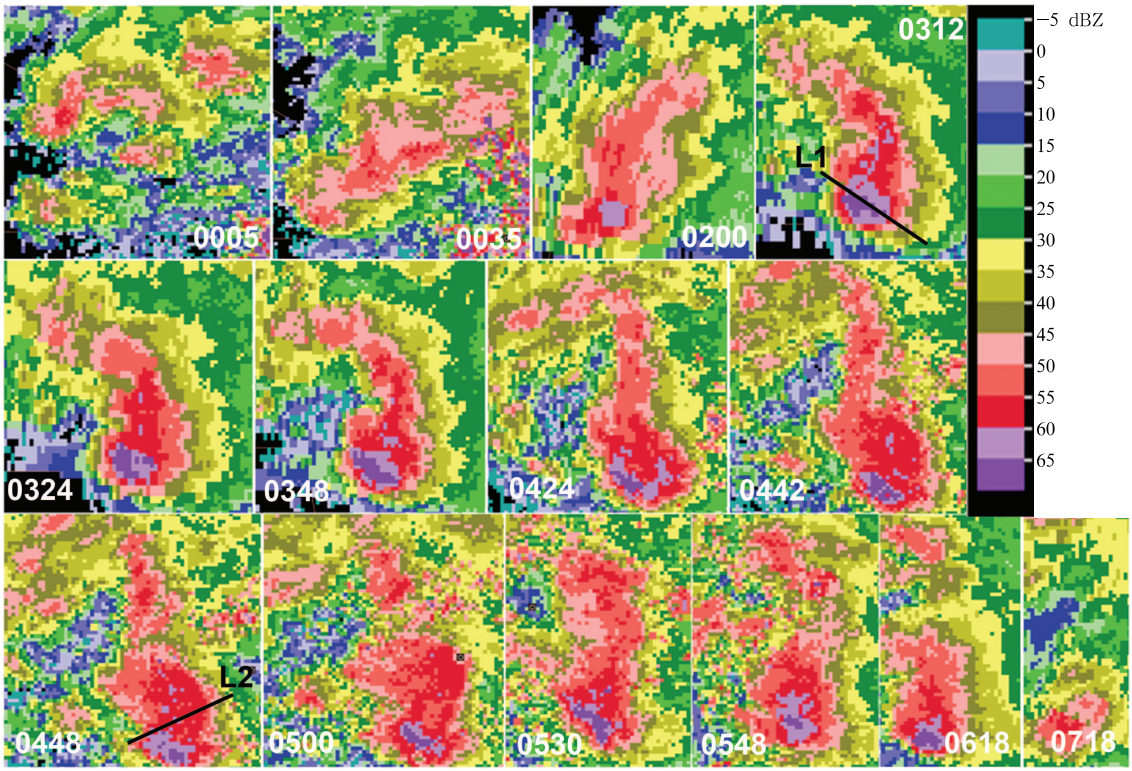

Fig. 4. Composite radar reflectivity factors from 0005 to 0718 UTC 17 April 2011. The first two figures on the top panel are observed by the radar at Wuzhou; the remainders are observed by the radar at Guangzhou.

southwesterly. A clear boundary formed in the opposite direction of the mean flow and thread-like tails formed in the same direction as the mean flow as the thunderstorm anvil expanded. The shadow faded after 0500 UTC 17 April due to a decrease in the height of the cloud top associated with the weakening of the DPMCS.

The radar-observed echo was concentrated mainly in the eastern part of the DPMCS. The evolution of SRE area can be divided into two stages: a high-precipitation supercell stage (0005–0442 UTC 17 April) and a non-supercell stage (0448–0718 UTC 17 April). During the non-supercell stage, the radar echo was sequentially observed to be kidney-shaped, foot-shaped, and ordinary single cell.

2.1 Characteristics of the supercell stage

At 0005 UTC 17 April, several single-cell convective storms formed near Wuzhou in Guangxi Region (Fig. 4). At 0035 UTC, these single-cell storms merged to form a line echo with a southwest–northeast orientation. At 0200 UTC, the line echo moved into Guangdong Province (Fig. 1) and bent into a bow shape. Radar reflectivity in the echo core in the south of the SRE area reached 60 dBZ (Fig. 4). The strong gradient of reflectivity in this area at the 2.4° elevation angle (area indicated by the arrows in Fig. 5a), called the low-level inflow notch, was coincident with radial velocity convergence at the 2.4° elevation angle (Fig. 5c) and the location of the SRE core at the 9.9° elevation angle (Fig. 5b). This indicates that an echo was located directly above the weak echo region (WER) at this time. The low-level inflow notch was sustained and accompanied by a mesovortex during the evolution stage of the bow-echo configuration supercell. The radial velocity in the SRE core area was divergent in the middle troposphere (Fig. 5d), illustrating that the low-level inflow created updrafts that diverged upon reaching the middle troposphere. At 0312 UTC, an echo vault was observed in the profile across the SRE area, and the storm top was located above the bounded WER (Fig. 6a). Both of these

features are classic characteristics of supercells.

At 0324 UTC, the north part of the bow echo took the shape of a left parenthesis (Fig. 4). At 0348 UTC, this left-parenthesis-shaped echo disappeared and the SRE area returned to a bow shape. The north part of the bow echo was spiral shaped at this point due to

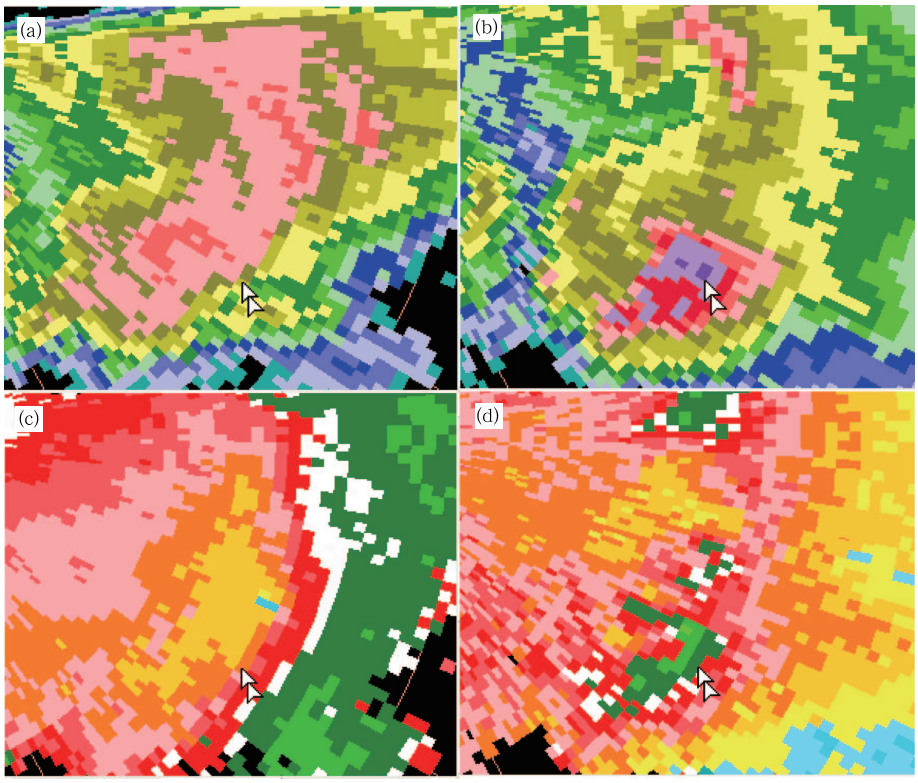

Fig. 5. Reflectivity factor (a, b) and radial velocity (c, d) observed by the Guangzhou radar at 0200 UTC 17 April 2011. (a, c) 2.4° elevation and (b, d) 9.9° elevation. Arrows point to the same horizontal position; the altitude of the indicated position is approximately 1.8 km at 2.4° elevation and 6.7 km at 9.9° elevation. See the color bars in Fig. 6.

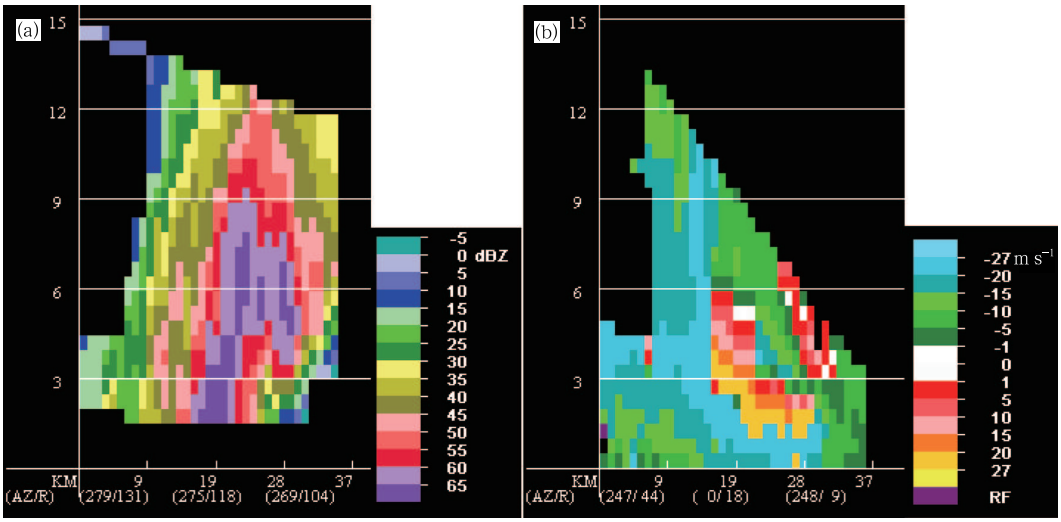

Fig. 6. (a) Cross-section of radar reflectivity factor along L1 (see Fig. 4) observed by the Guangzhou radar at 0312 UTC 17 April 2011. (b) Cross-section of radial velocity along L2 (see Fig. 4) at 0448 UTC 17 April 2011.

the influence of a mesovortex. At 0424 UTC, the radial velocity was divergent in the northern part of the bow echo at the 1.5°, 2.4°, and 3.4° elevation angles. This divergence strengthened with time, and a meso-anticyclone appeared in the echo at the 1.5° elevation angle at 0442 UTC. The northern end of the bow echo weakened and disappeared as the divergence strengthened.

Heavy rainfall occurred in the area that the SRE passed during the evolution of the bow-echo configuration supercell (Fig. 7a); this is a classic characteristic of a high-precipitation supercell (Moller et al., 1994). Moreover, frequent lightning occurred in the heavy rainfall area. Previous studies indicate that high-precipitation supercells often induce dangerous hail, gales, and heavy rainfall, but do not generally produce severe tornados (Johns, 1993). High-precipitation supercells can develop in a variety of ways; development of a bow-echo configuration high-precipitation supercell often leads to surface gales (> 25 m s^{-1}) and large hail (diameter > 1.9 cm), and such systems always move along the surface boundaries (front, dry line) (Klimowski et al., 2004). A WER persisted in the rear flank of this high-precipitation supercell throughout its evolution (Fig. 4). This WER was related to the rear inflow in the middle troposphere.

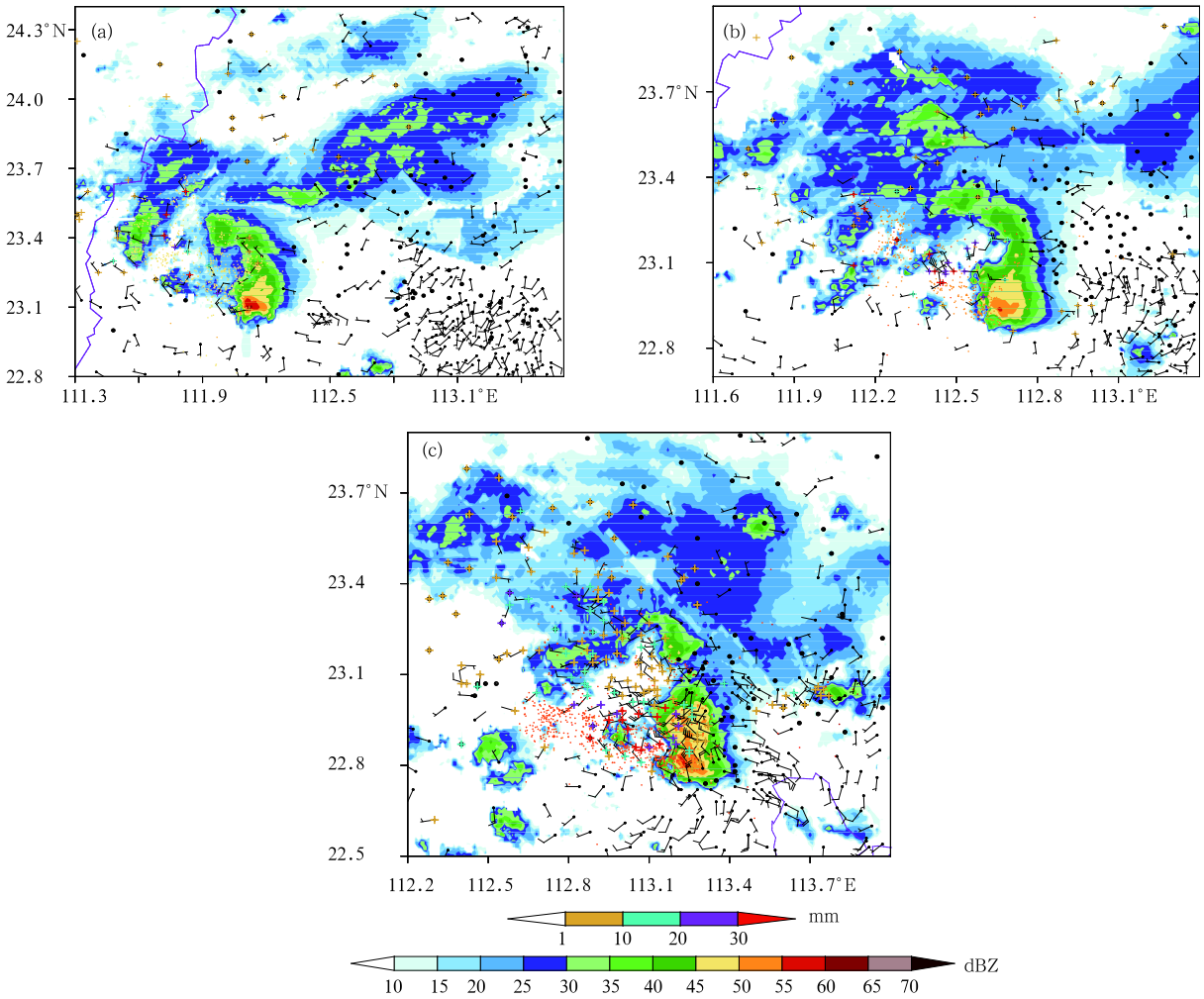

Fig. 7. Hourly precipitation (crosses of different colors represent different precipitation levels; mm), surface wind (each full barb represents 4 m s^{-1}), lighting strikes (yellow dots), and radar reflectivity factor (shadings; dBZ) at 4-km altitude at (a) 0300 UTC, (b) 0400 UTC, and (c) 0500 UTC 17 April 2011.

2.2 Characteristics of the non-supercell stage

At 0448 UTC, the bow echo broke in the middle section (Fig. 4). Mid-altitude radial convergence (MARC) occurred on the profile across line L2 (Fig. 6b), which is indicative of the existence of gales at the ground level (Przybylinski, 1995). At 0500 UTC, the SRE area in the southern part of the system became kidney shaped, with a WER in the rear region and an overhanging echo along the arc-shaped eastern edge. Reflectivity factors in this kidney-shaped area were radialized at the 0.5° elevation angle prior to evolving into a foot-shaped echo at 0530 UTC. Radialized echoes and foot-shaped echoes are both characteristic of downbursts. The foot-shaped echo broke into two parts at 0548 UTC. The northern part weakened gradually while the southern part evolved into an ordinary single cell. The reflectivity of the SRE area in this ordinary single cell increased at 0618 UTC before decreasing at 0630 UTC.

3. The formation of gales at ground level during different stages

3.1 Supercell stage

The outflow boundary of a convective storm, usually indicated by a fine line on weather radar images, is a storm-scale boundary that separates the storm from the surrounding air. The outflow boundary is sometimes very close to the storm. Growing separation between the outflow boundary and the storm indicates that the storm is weakening. The outflow boundary of the storm analyzed here was located very close to the storm, especially during the supercell stage when a convergence line of radial velocity was located near the southeastern leading edge of the SRE area (see examples in Fig. 8c).

The maximum radial velocity in the lower troposphere occurred in the eastern part of the bow echo. Some velocity ambiguity existed at the 0.5° elevation at 0312 UTC (Fig. 8a), when the center of negative velocity reached –31 m s^{-1} approximately 1.9 km above the ground at the apex of the bow. The maximum negative velocity at the 2.4° elevation angle was also –31 m s^{-1}, approximately 5.9 km above the ground near the rear inflow notch of the bow echo (Fig. 8b). This rear inflow jet can dive rapidly toward the ground, creating strong downdrafts and straight-line winds. The radial velocity convergence line in the middle troposphere was located to the west of the radial velocity convergence line in the lower troposphere (Figs. 8c and 8d), indicating that the existence of a westward-tilting updraft at the eastern leading edge of the bow echo. Starting at 0354 UTC, the convergence line lengthened and departed from the SRE area.

3.2 Non-supercell stage

The convergence line to the south of the bow-echo configuration supercell approached the SRE beginning at 0430 UTC, while the convergence line to the north of the supercell moved further from the SRE. As indicated in Section 2, the northern part later disappeared while the southern part developed into first kidney-shaped and then foot-shaped echoes. The characteristic of the convergence at this time differed from that during the previous stage. For example, the convergence line to the south of the SRE was observed only at the 0.5° elevation angle at 0430 UTC; the radial velocity was divergent in the corresponding area at the 6.0° elevation angle. In fact, this pattern of convergence at low levels and divergence above was first observed at 0424 UTC. The radial velocity maximum no longer tilted westward at this time, with maximum negative velocities of –31 m s^{-1} at the 0.5° elevation angle (approximately 0.6 km above the ground) and –37 m s^{-1} at the 1.5° elevation angle (approximately 1.3 km above ground). The maximum absolute velocity at immediately subsequent times always exceeded 31 m s^{-1}, indicating that ground-level wind speeds were very high (generally, wind speeds in excess of 20 m s^{-1} within 1 km of the ground can be considered very high). The SRE was located in a radar blind zone at 0506 UTC. From 0512 to 0606 UTC, the maximum radial velocity near 1-km altitude was 23 m s^{-1}. After 0612 UTC, the radar echo of the SRE was located more than 60 km from the radar; accordingly, the characteristics of the system at 1-km altitude were not captured by the radar at the 0.5° elevation angle. Based on the apparent decay of the SRE at this time, it is likely that the surface wind speed was decreasing.

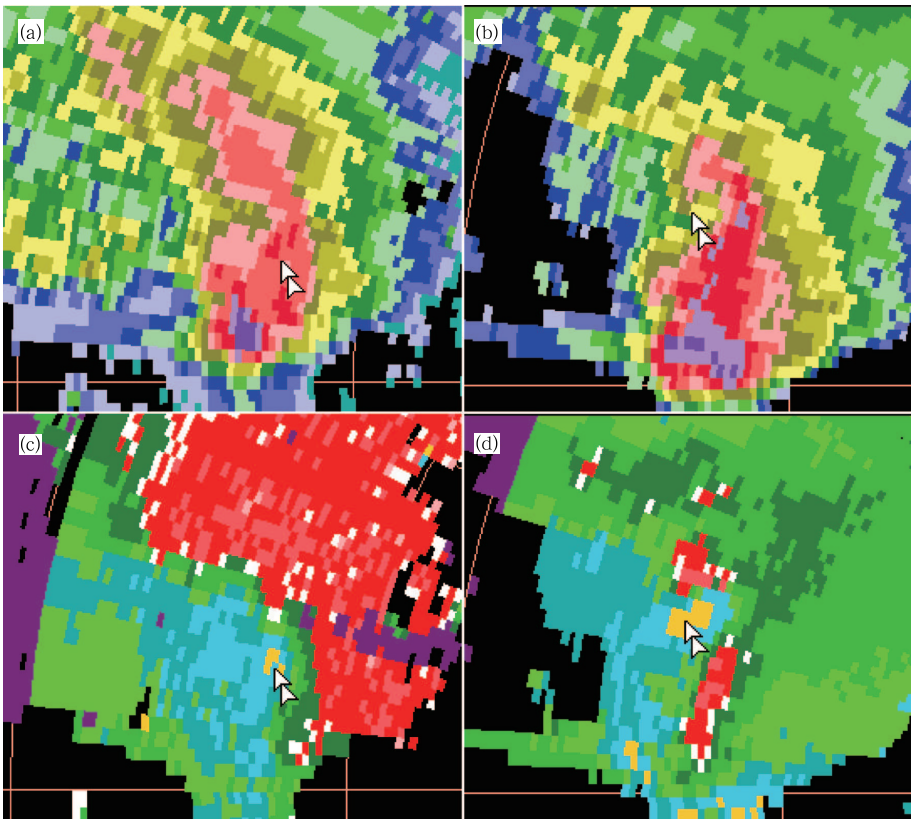

Fig. 8. Reflectivity factor (a, b) and radial velocity (c, d) observed by the Guangzhou radar at 0312 UTC 17 April 2011. (a, c) 0.5° elevation angle (the area indicated by the arrow is approximately 112 km from the radar and 1.9 km in altitude) and (b, d) 2.4° elevation angle (the area indicated by the arrow is approximately 116.5 km from the radar and 6 km in altitude). See the color bars in Fig. 6.

From 0524 to 0536 UTC, the retrieved radial velocities were ambiguous to the southeast of the SRE core at the 0.5° elevation angle (approximately 0.5 km), with a maximum outflow speed of 31 m s^{-1}. At 0530 UTC, the flow to the northwest of the SRE core was oriented towards the radar (Fig. 9a), indicating divergence of radial velocity near the SRE core. This divergence was distributed vertically between the 0.5° and 2.4° elevation angles; that is, the flow near the SRE core was divergent below 1.2-km altitude. Meanwhile, the flow was convergent at approximately 5-km altitude (Fig. 9b). Review of the radar images from earlier in the day indicates that this pattern of divergence in the boundary layer and convergence in the middle troposphere began at 0500 UTC. The divergence in the boundary layer was strongest at 0530 UTC. The horizontal distance between the positive and negative velocity centers was approximately 8 km, with a difference in velocity of 43 m s^{-1} (Fig. 9a). The boundary layer divergence weakened and the divergent area departed from the SRE core after 0530 UTC, disappearing altogether after 0548 UTC. The convergence in the middle troposphere disappeared after 0536 UTC. The intensification of the divergence in the boundary layer from 0500 to 0530 UTC accompanied a growth and strengthening of the SRE core at the 0.5° elevation angle. These characteristics indicate the occurrence of a downburst between 0500 and 0548 UTC along with the sinking of the SRE core.

The SRE area evolved into an ordinary single cell storm by 0600 UTC. The core of this storm was still located in the southern portion of the SRE area. An area of divergence developed again around the SRE core at approximately 1-km altitude. The difference

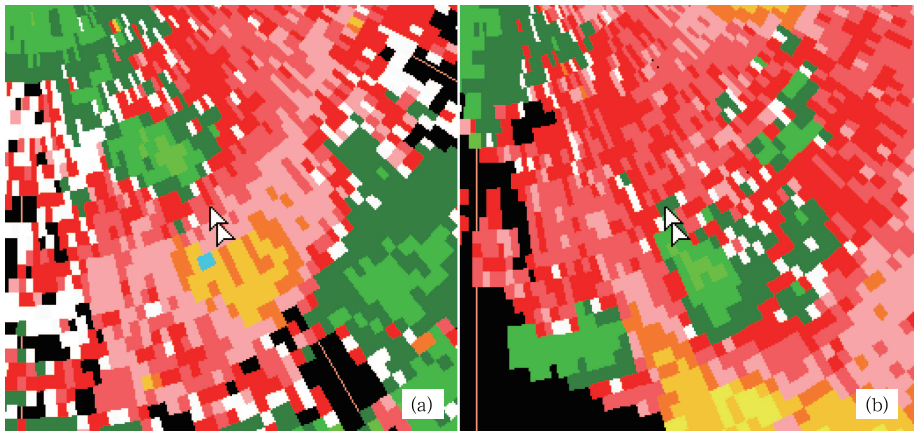

Fig. 9. Radial velocity observed by the Guangzhou radar at 0530 UTC 17 April 2011 along (a) the 0.5° elevation angle (the area indicated by the arrow is approximately 0.5 km in altitude) and (b) the 9.9° elevation angle (the area indicated by the arrow is approximately 5.4 km in altitude). The arrows in (a) and (b) indicate the same horizontal position approximately 30 km from the radar. See the color bar in Fig. 6b.

in azimuth angle between the positive and negative velocity centers was approximately 2°, while the difference in velocity was approximately 30 m s^{-1}. This same horizontal area contained convergence between 2- and 4-km altitude. Relative to the first downburst, the level of the convergence was lower and the magnitude of the divergence was smaller. The area of negative velocity grew in size after 0600 UTC but the magnitude of the divergence did not change, implying that an outward spread of the downdraft at lower levels. At 0630 UTC, the radar reflectivity in the echo core at the 0.5° elevation angle increased suddenly to more than 65 dBZ. The layer of divergence extended upward to approximately 2.7 km at this time, indicating that a weaker downburst and a deeper divergent layer accompanied the sinking of the core. The single cell echo weakened and split into several smaller single cells at 0642 UTC. The maximum single cell echo (53 dBZ) was located in the south, and the maximum horizontal scale was approximately 15 km.

At 0648 UTC, the maximum reflectivity of the biggest single cell increased to 57 dBZ. Divergence was observed around the SRE area; however, the area of this divergence was smaller than the two previous downbursts. The difference between the centers of positive and negative velocity near 1.5 km altitude was approximately 14 m s^{-1}. Convergence was observed at 3.5 and 5 km altitude. The divergence observed at the 0.5° elevation angle weakened at subsequent observation times. After 0706 UTC, the SRE was located more than 110 km from the radar; thus the radar observations could not capture the wind distribution below 1 km.

Above all, the causes of the gale can be divided into two stages. The first stage corresponded to the bow-echo configuration supercell stage, in which the gale was mainly attributable to a sinking rear inflow jet. The second stage corresponded to the non-supercell stage, in which the gale was mainly attributable to downbursts. Three downbursts could be identified in the radar images.

Previous research has indicated that straight-line windstorms can be related to mesovortices (Trapp and Weisman, 2003). As mentioned in Section 2, two classes of mesovortex occurred during the bow-echo configuration supercell stage. One mesovortex was related to the low-level inflow notch while the other was related to the spiral-shaped echo in the northern part of the supercell. However, the gale was observed primarily at the eastern bulge of the bow echo. The differences in the locations of the mesovortices and the gale imply that the gale was independent of the mesovortices.

The two categories of gale can also be differen-

tiated in the satellite images (Fig. 3). From 0000 to 0300 UTC 17 April, several bands of arc clouds were observed to the south of the DPMCS. These arc clouds were most prominent at 0300 UTC, when they were located in the area corresponding to the radar echoes (figure omitted). The arc clouds were related to the outflow boundary of the bow echo. The arc clouds weakened and disappeared starting at 0400 UTC, likely due to downbursts, and were replaced by less-organized clouds.

4. Environmental conditions

A low-level cyclonic shear line oriented in the southwest–northeast direction (Figs. 10a and 10b) contributed to the convergence and upward motion of airflow. There was no obvious trough at 500 hPa, nor was there a synoptic-scale cyclone at the surface (Figs. 10 and 11), indicating that the synoptic-scale forcing was not strong (Evans and Doswell III, 2001). The conditions that led to the windstorm are discussed in the following sections.

4.1 Unstable energy and strong vertical wind shear

The DPMCS covered Wuzhou in Guangxi Region at 0000 UTC 17 April. A sounding (Fig. 12) taken by Wuzhou station at this time shows the existence of a dry layer in the middle troposphere. The convective available potential energy (CAPE) was 1184 J, and the convective inhibition (CIN) was 0 J. Both of these values indicate a favorable environment for convection. The 0℃ temperature level was located at 600 hPa. This vertical location was lower than 12 h

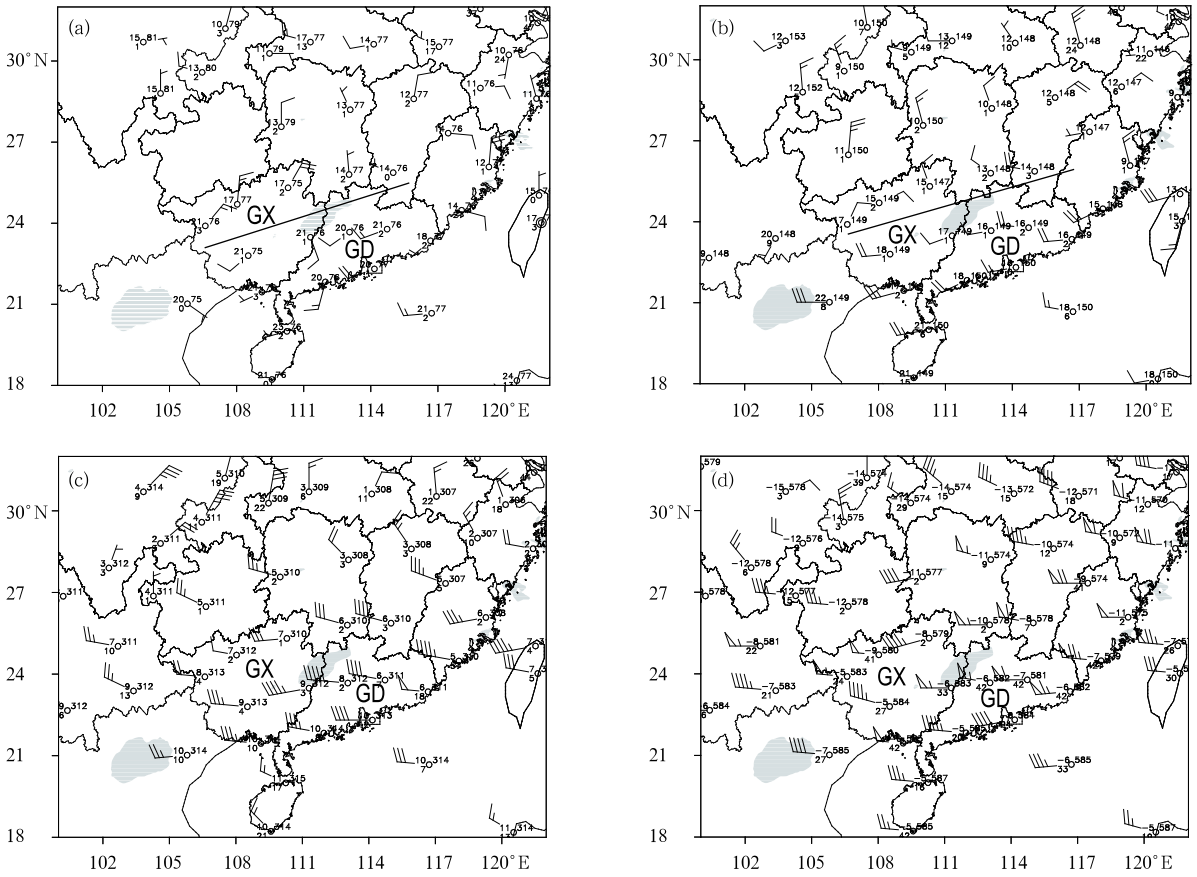

Fig. 10. Geopotential height (10 gpm), temperature (℃), wind field (each barb on a bar represents 4 m s^{-1}), and dew point depression (℃) at 0000 UTC 17 April 2011 at (a) 925 hPa, (b) 850 hPa, (c) 700 hPa, and (d) 500 hPa. The shaded areas represent convective cloud clusters. The lines at 925 and 850 hPa indicate shear lines of horizontal wind. GX means Guangxi Region and GD denotes Guangdong Province.

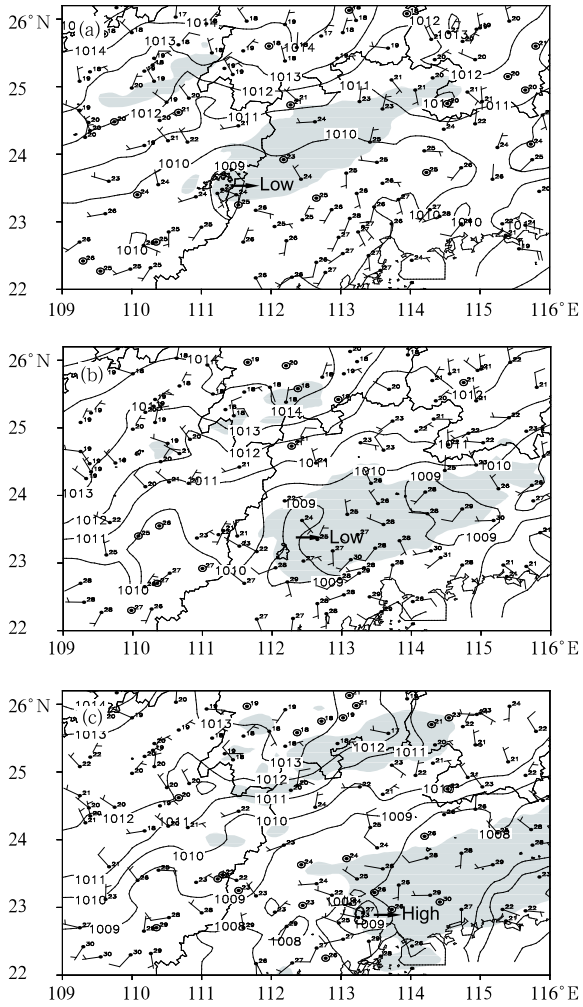

Fig. 11. Sea-level pressure (grey contours; hPa), surface winds (each barb on a bar represents 4 m s^{-1}), temperature (digits; ℃), radar reflectivity factor at 4 km (black contours; 45 dBZ), and convective cloud clusters (shaded area) at (a) 0100 UTC, (b) 0300 UTC, and (c) 0500 UTC 17 April 2011.

before and indicates favorable conditions for hail to fall to the ground. The horizontal wind rotated clockwise with increasing height, implying the existence of warm thermal advection and increasing unstable energy of the air column. The vertical wind shear between 0- and 3-km altitude was approximately 22 m s^{-1}, while that from 0- to 6-km altitude was approximately 31 m s^{-1}. These strong vertical wind shears supported the formation of supercell storm, bow echo, low-level mesovortex, and strong outflow at lower levels (Gilmore and Wicker, 1998; Trapp and Weisman, 2003).

The closest sounding station to the windstorm in Guangdong was Qingyuan station (23.70°N, 113.08°E); however, this station was located 100 km from the DPMCS at 0000 UTC 17 April. The sounding at Qingyuan station also indicated a dry layer in the middle troposphere and strong vertical wind shear, but the CAPE was 553 J, much smaller than that observed at Wuzhou station.

4.2 Initiation effect of surface boundaries

From 2300 UTC 16 April to 0300 UTC 17 April, the 1010-hPa isobar at sea level gradually moved southward (Fig. 11). Northerly winds were dominant to the north of the 1010-hPa isobar, while southerly winds were dominant approximately 50 km south of this isobar. The temperature difference between the north and the south was apparent. The southward motion of northerly winds indicates that the cold air mass was stronger than the warm air mass. The iso-

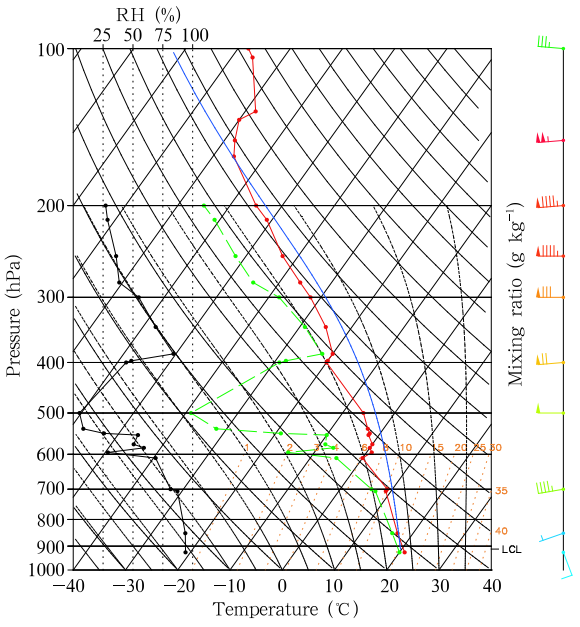

Fig. 12. Skew T-log$p$ diagram observed by Wuzhou station (23.48°N, 111.30°E) at 0000 UTC 17 April 2011. The red and green curves are the profiles of environmental temperature and dew-point temperature, respectively. The blue curve is the temperature profile of an air parcel lifted adiabatically. The black curve is the profile of relative humidity.

bar ceased its southward progression after 0300 UTC 17 April, indicating that a balance was established between the cold and warm air masses. A persistent low was observed in the western part of the DPMCS throughout the development of the bow-echo configuration supercell (from 0000 to 0300 UTC 17 April). The storm moved southward with the southward progression of the cold front, a classic characteristic of high precipitation supercells (Klimowski et al., 2004). The uplift induced by the front may be the main mechanism underlying the development of the bow-echo configuration supercell. The front and the bow-echo configuration supercell both weakened after 0300 UTC.

A surface wind convergence line was maintained during the derecho event at the front area of the SRE (Fig. 7) in the western part of the DPMCS (Fig. 11). At 0100 and 0200 UTC 17 April, there was convergence of northerly wind and southerly wind along the southeastern edge of the SRE area. This convergence area extended between 0300 and 0400 UTC, and was located in the northern part of the SRE at 0600 UTC.

4.3 The dry layer in the middle troposphere

The dew point depressions at 925 and 850 hPa were approximately 1 to 2℃, which is near saturation (Fig. 10). Westerly winds were dominant at 700 hPa in the area close to the DPMCS. The atmosphere in the vicinity of the DPMCS was near saturation, while the atmosphere along the coast of Guangdong and Guangxi was very dry. The dew point depression in this latter region was higher than 8℃, indicating a strong contrast between wet and dry air to the south of the DPMCS. At 500 hPa, the atmosphere to the west and south of the DPMCS was very dry, with a maximum dew point depression of 42℃. In summary, the atmosphere was very wet in the boundary layer but very dry in the middle and upper troposphere to the west and south of the DPMCS. This moisture configuration was beneficial to the formation of strong low-level outflow (Gilmore and Wicker, 1998).

4.4 Downdraft convective available potential energy

Downdraft convective available potential energy (DCAPE) is the maximum increase in kinetic energy that can result from evaporative cooling of the air within a hypothetical parcel as it descends from some source height to the ground (Gilmore and Wicker, 1998). This index has some limitations; for example, the air mass is assumed not to mix with the surrounding environment during its descent, but the index has been widely used in research and operational work. DCAPE has been defined as (Gilmore and Wicker, 1998):

$$\mathrm{DCAPE} = g\int_{z_{\mathrm{sfc}}}^{z_n}\frac{\bar{\theta}(z)-\theta(z)}{\bar{\theta}(z)}\mathrm{d}z,$$

where z_n is the source height from which the parcel starts to descend, z_{sfc} is the height of the ground surface, $\bar{\theta}(z)$ and $\theta(z)$ are the potential temperatures of the environment and the saturated downdraft parcel, respectively, and g is the acceleration of gravity. The maximum DCAPE can be obtained by setting z_n as the level of the minimum pseudo-equivalent potential temperature. At 0000 UTC 17 April, the DCAPE and z_n at Qingyuan station were 1005 J kg^{-1} and 4700 m, respectively, while those at Wuzhou station were 812 J kg^{-1} and 4440 m, respectively. The downbursts occurred 4 h after 0000 UTC, and conditions that favored an increase in DCAPE (e.g., strengthening of the dry intrusion) may have occurred during this 4-h period.

4.5 Temperature lapse rate of the environment

At 0000 UTC, the temperature profile below 650 hPa in Wuzhou was steeper than the wet adiabatic lapse rate (Fig. 12). The temperature of a descending air parcel was therefore lower than that of the environmental atmosphere, which contributed to maintaining the negative buoyancy of downdraft.

5. Conclusions and discussion

In this paper, radar, satellite, and surface observation data were used to analyze a derecho event in Guangdong Province on 17 April 2011. The main conclusions are as follows.

(1) The derecho can be divided into two stages according to differences in the characteristics of the radar echo: a supercell stage and a non-supercell stage. The

supercell in the first stage was a high-precipitation supercell in a bow-echo configuration. During this stage, high precipitation in the SRE area was accompanied by frequent lightning, while precipitation was relatively light in the associated stratiform precipitation area. A mesovortex formed at the weak echo region in the lower troposphere associated with the low-level inflow notch; this mesovortex was enclosed within the area of high precipitation. Another mesovortex formed in a spiral-shaped echo area in the northern part of the bow echo. A V-shaped notch was observed in the rear region, which was associated with a downdraft. The high-precipitation supercell occurred in an environment with ample water vapor in the lower layers and a low lifting condensation level, and moved in tandem with the surface front. All of these characteristics are classically associated with high-precipitation supercells (Moller et al., 1994).

(2) The causes of the gales that occurred during the two stages were also different. The sinking rear inflow jet led to the gale in the first stage; this gale was weaker than the gales induced by downbursts during the second stage. The SRE core sank in conjunction with the occurrence of the downbursts, and the wind field was divergent in the lower troposphere and convergent in the middle troposphere.

(3) A dry layer in the middle troposphere, moderate values of DCAPE and CAPE, strong vertical wind shear, a steep temperature lapse rate relative to the moist adiabat, and horizontal wind shear in the lower troposphere all promoted the initiation of the DPMCS.

(4) The causes and structure of this derecho had many similarities with previously observed progressive derechos in Europe and North America. For example, the storm moved in tandem with a front, the bow echo was oriented nearly perpendicular to the mean flow, and the gales were distributed in the bulging portion of the bow echo (Johns and Hirt, 1987). The thermal boundaries also contributed significantly to the derecho, which was similar to some previous studies (Bentley et al., 2000). Not all of the characteristics of this derecho were similar to those observed in Europe and North America, however. The synoptic-scale forcing was not strong according to the classification of Evans and Doswell III (2001), since the system lacked both an advancing high-amplitude midlevel trough and an accompanying strong surface cyclone; however, the vertical wind shear was very strong, a characteristic typical of strong-forcing archetype derechos (Doswell III and Evans, 2003). Weak-forcing archetype and hybrid derechos are typically associated with very high values of CAPE and DCAPE, but CAPE and DCAPE in this case were both much less than 2000 J. A more detailed and accurate comparison between derechos in China and those in other parts of the world will require the study and statistical analysis of additional cases.

REFERENCES

Ashley, W. S., T. L. Mote, and M. L. Bentley, 2005: On the episodic nature of derecho-producing convective systems in the United States. *Int. J. Climatol.*, **25**, 1915–1932.

Bentley, M. L., and T. L. Mote, 1998: A climatology of derecho-producing mesoscale convective systems in the central and eastern United States, 1986–1995. Part I: Temporal and spatial distribution. *Bull. Amer. Meteor. Soc.*, **79**, 2527–2540.

——, ——, and S. F. Byrd, 2000: A synoptic climatology of derecho producing mesoscale convective systems in the north-central plains. *Int. J. Climatol.*, **20**, 1329–1349.

Chen Yeguo, Nong Mengsong, Huang Haihong, et al., 2009: Numerical simulation and analysis on a strong squall line in South China. *Meteor. Mon.*, **35**(9), 29–37. (in Chinese)

Coniglio, M. C., and D. J. Stensrud, 2004: Interpreting the climatology of derechos. *Wea. Forecasting*, **19**, 595–605.

Doswell III, C. A., and J. S. Evans, 2003: Proximity sounding analysis for derechos and supercells: An assessment of similarities and differences. *Atmos. Res.*, (67–68), 117–133.

Evans, J. S., and C. A. Doswell III, 2001: Examination of derecho environments using proximity soundings. *Wea. Forecasting*, **16**, 329–342.

Fujita, T. T., 1981: Tornadoes and downbursts in the context of generalized planetary scales. *J. Atmos. Sci.*, **38**(8), 1511–1534.

Gatzen, C., 2004: A derecho in Europe: Berlin, 10 July 2002. *Wea. Forecasting*, **19**, 639–645.

Gilmore, M. S., and L. J. Wicker, 1998: The influence of midtropospheric dryness on supercell morphology and evolution. *Mon. Wea. Rev.*, **126**, 943–958.

Hinrichs, G., 1888: Tornadoes and derechos. *Amer. Meteor. J.*, **5**, 306–317, 341–349.

Johns, R. H., 1993: Meteorological conditions associated with bow echo development in convective storms. *Wea. Forecasting*, **2**, 32–49.

——, and W. D. Hirt, 1987: Derechos: Widespread convectively induced windstorm. *Wea. Forecasting*, **2**, 32–49.

Klimowski, B. A., M. R. Hjelmfelt, and M. J. Bunkers, 2004: Radar observations of the early evolution of bow echoes. *Wea. Forecasting*, **19**, 727–734.

Moller, A. R., C. A. Doswell III, M. P. Foster, et al., 1994: The operational recognition of supercell thunderstorm environments and storm structures. *Wea. Forecasting*, **9**, 327–347.

Przybylinski, R. W., 1995: The bow echo: observations, numerical simulations and severe weather detection methods. *Wea. Forecasting*, **10**, 203–218.

Sun Hulin, Luo Yali, Zhang Renhe, et al., 2011: Analysis on the mature-stage feature of the severe squall line occurring over the Yellow River and Huaihe River basins during 3–4 June 2009. *Chinese J. Atmos. Sci.*, **35**(1), 105–120. (in Chinese)

Trapp, R. J., and M. L. Weisman, 2003: Low-level mesovortices within squall lines and bow echoes. Part II: Their genesis and implications. *Mon. Wea. Rev.*, **131**, 2804–2823.

Wang Jun, Gong Dianli, Diao Xiuguang, et al., 2011: Case study of bow echo, severe convective storm and merger process. Part I: Taking single Doppler radar data as a case. *Plateau Meteor.*, **30**(4), 1067–1077. (in Chinese)

Yao Yeqing, Yu Xiaoding, Zhang Yijun, et al., 2008: Analysis on a typical squall line case with Doppler weather radar data. *Plateau Meteor.*, **27**(2), 373–381. (in Chinese)